J|A|C|S
ARTICLES
Published on Web 08/27/2003

Singular Crystalline β'-Layered Topologies Directed by Ribbons of Self-Complementary Amide···Amide Ring Motifs in [EDT-TTF-$(CONH_2)_2$]$_2$X (X = HSO_4^-, ClO_4^-, ReO_4^-, AsF_6^-): Coupled Activation of Ribbon Curvature, Electron Interactions, and Magnetic Susceptibility

Stéphane A. Baudron,[†] Narcis Avarvari,[†] Patrick Batail,*[,†] Claude Coulon,[‡] Rodolphe Clérac,[‡] Enric Canadell,[§] and Pascale Auban-Senzier[||]

Contribution from Chimie Inorganique, Matériaux et Interfaces, FRE 2447, CNRS−Université d'Angers, Bâtiment F, 2 Boulevard Lavoisier, 49045 Angers, France, Centre de Recherches Paul Pascal, Avenue du Dr Schweitzer, 33600 Pessac, France, Institut de Ciencia de Materials, Consejo Superior de Investigaciones Científicas, Campus de la UAB, E-08193 Bellaterra, Spain, and Laboratoire de Physique des Solides, UMR 8502 CNRS−Université Paris-Sud, Bâtiment 510, 91405 Orsay, France

Received April 14, 2003; E-mail: patrick.batail@univ-angers.fr

Abstract: The deliberate design of a series of single crystals of conducting two-dimensional radical cation salts of *o*-bis(amide)-appended ethylenedithiotetrathiafulvalene, β'-[EDT-TTF-$(CONH_2)_2$]$_2$X (X = HSO_4^-, ClO_4^-, ReO_4^-, or AsF_6^-) and of their parent monocomponent solid EDT-TTF-$(CONH_2)_2$ is demonstrated and allows us to reach a level of prediction of the structure of molecular conductors. Their conductivity is activated with a gap of 1650 K and a sizable room-temperature conductivity of 0.15 S·cm^{-1} (for X = ClO_4^-) and a singular spin susceptibility for a β'-type salt that, in addition, changes very remarkably with the anion. The key design element is that of a recurrent, puckered ribbon constructed out of self-complementary, hydrogen-bonded amide···amide ring motifs whose minute modulations of curvature and shape throughout the series have been shown to correlate to very remarkable differences in the intrastack $\beta_{HOMO-HOMO}$ interaction energies and changes in the density of states at the Fermi level and on to important differences of spin susceptibility behavior in a system where electron correlations are significant. The coupled activation of structure, electron interactions, and magnetic susceptibility discovered and discussed throughout the paper is unprecedented and is seen as a genuine expression of interfacial hydrogen-bond interactions onto the collective electronic properties.

Introduction

Despite high expectations expressed by practitioners of many fields branching out of supramolecular chemistry, our present ability to direct the arrangement of molecules in crystalline solids[1−6] and control their collective electronic properties[6−8] is still in its infancy. In the case of hydrogen bonding, a valuable strategy has been to search a posteriori for recurrent patterns within the large database of numerous crystal structures of molecular solids;[2,5] hence, the vaunted capacity of carboxylic acids or amides to produce order through self-complementary association. Amides have recently been introduced in tetrathiafulvalene- (TTF-) based materials.[6,9−11] Interestingly, a templating effect of the inorganic counteranion has been revealed[6] in radical cation salts of the primary amide-appended (ethylenedithio)tetrathiafulvalene, EDT-TTF-$CONH_2$. For example, electrocrystallization[12] with ReO_4^- affords a metallic 2:1 salt, [EDT-TTF-$CONH_2$]$_2$$ReO_4$, and the same experiment with isosteric AsF_6^- affords the 6:1 salt, [EDT-TTF-$CONH_2$]$_6$$AsF_6$. In both instances, anion recognition takes over and there is no

* Corresponding author: Tel +33 2 41 73 52 64; fax +33 2 41 73 50 11.
[†] FRE 2447, CNRS−Université d'Angers.
[‡] Centre de Recherches Paul Pascal, Pessac.
[§] ICMAB−CSIC.
[||] UMR 8502 CNRS-Université Paris-Sud.

(1) Lehn, J.-M. *Proc. Natl. Acad. Sci. U.S.A.* **2002**, *99*, 4763−4768.
(2) Desiraju, G. R. *Angew. Chem., Int. Ed. Engl.* **1995**, *34*, 2311−2327.
(3) Allen, F. H.; Motherwell, W. D. S.; Raithby, P. R.; Shields, G. P.; Taylor, R. *New J. Chem.* **1999**, 25−34.
(4) Aakeröy, C. B.; Beatty, A. M.; Helfrich, B. A. *J. Am. Chem. Soc.* **2002**, *124*, 14425−14432.
(5) Sarma, J. A. R. P.; Desiraju, G. R. *Cryst. Growth Des.* **2002**, *2*, 93.
(6) Heuzé, K.; Fourmigué, M.; Batail, P.; Canadell, E.; Auban-Senzier, P. *Chem. Eur. J.* **1999**, *5*, 2971−2976.
(7) Devic, T.; Evain, M.; Moëlo, Y.; Canadell, E.; Auban-Senzier, P.; Fourmigué, M.; Batail, P. *J. Am. Chem. Soc.* **2003**, *125*, 3295−3301 and references therein.
(8) Canadell, E.; Ordejón, P.; Artacho, E.; Sánchez-Portal, D.; García, A.; Soler, J. *J. Mater. Chem.* **2001**, *11*, 1−10.
(9) Heuzé, K.; Fourmigué, M.; Batail, P. *J. Mater. Chem.* **1999**, *9*, 2373−2379.
(10) Heuzé, K.; Mézière, C.; Fourmigué, M.; Batail, P.; Coulon, C.; Canadell, E.; Auban-Senzier, P.; Jérome, D. *Chem. Mater* **2000**, *12*, 1898−1904.
(11) Boyd, A. S. F.; Cooke, G.; Duclairoir, M. A.; Rotello, V. M. *Tetrahedron Lett.* **2003**, *44*, 303.
(12) Batail, P.; Boubekeur, K.; Fourmigué, M.; Gabriel, J.-C. *Chem. Mater.* **1998**, *10*, 3005−3015.

Chart 1

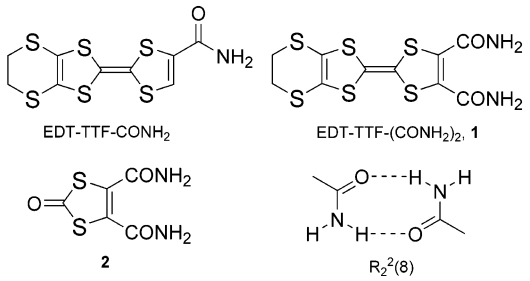

evidence for the classical, self-complementary amide···amide $R_2^2(8)$ motif [13] typically observed in the parent monomolecular solid. This is surprising since a recent thorough Cambridge Structural Database analysis has revealed that the probability for this type of motif is 80% for monoamide and reaches 95% for diamide.[3] It was therefore felt that the use of diamide ethylenedithiotetrathiafulvalene, EDT-TTF-$(CONH_2)_2$, **1** (Chart 1), may allow us to take advantage of recurrent motifs for the directed construction of molecular solids while maintaining additional anion templating opportunities. In particular, by use of EDT-TTF-$(CONH_2)_2$, the $R_2^2(8)$ motif should be present and may favor a robust arrangement of the π-donors. Moreover, the double functionality allows for a competition between inter- and intramolecular hydrogen bonding.

In this paper we report on the synthesis of **1**, analyze its crystal structure and that of a related compound, the corresponding dithiolone **2**,[14] and demonstrate that a common, robust pattern of self-complementary amide···amide hydrogen bonds directs the molecules to assemble within a two-dimensional topology, typical of conducting molecular solids. We also demonstrate that, when engaged in electrocrystallization experiments with single-charged anions to form single crystals of the title series, the robustness and adaptability of the former interfacial hydrogen-bond pattern prevail and direct the formation of the two-dimensional β'-topology, which constitutes a good example of crystal engineering in TTF-based materials.

Furthermore, the discovery that this novel series exhibits an activated conductivity but does not present the low-temperature antiferromagnetic ground state expected for β'-salts triggered the in-depth study reported herein where their diverse magnetic susceptibility behaviors are correlated to a singular topology of the density of states within the series and with minute differences in otherwise very similar structures, a likely and unprecedented expression of coupled activation of the pattern of intermolecular association and collective electronic behavior.

Experimental Section

Synthesis: 4,5-Ethylenedithio-4′,5′-Dicarbamoyltetrathiafulvalene 1. A CH_3CN (30 mL) solution of EDT-TTF-$(CO_2Me)_2$[15] (200 mg, 0.48 mmol) is reacted with an excess of ammonia in aqueous solution (25% w/w). After 24 h of stirring at room temperature, the resulting precipitate is filtered and recrystallized twice from tetrahydrofuran (THF), giving purple needles (136 mg, 73%), mp 266−267 °C. Anal. Calcd for $C_{10}H_8N_2O_2S_6$: C, 31.56; H, 2.12; N, 7.36; O, 8.41; S, 50.55. Found: C, 31.96; H, 2.08; N, 7.11; O, 8.66; S, 50.34. IR (KBr) 3380−3178 (NH_2), 1675−1662 (C═O) cm^{-1}; ^1H NMR (400 MHz, DMSO-d_6) δ 8.30 (br s, 2H, NH_2), 8.05 (br s, 2H, NH_2), 3.40 (s, 4H, CH_2-CH_2); ^{13}C NMR (100 MHz, DMSO-d_6) δ 161.42 (C═O), 134.08 (C−CO), 113.95−112.18−106.64 (C═C), 30.44 (CH_2–CH_2); UV/vis (THF) λ_{max} (ϵ) = 448 nm (1295 mol^{-1} dm^3 cm^{-1}); EI-MS *m*/*z* 380 ($M^{\bullet+}$, 100%).

Compound **2** was prepared as previously described[14] and recrystallized from acetonitrile. Anal. Calcd for $C_5H_4N_2O_3S_2$: C, 29.41; H, 1.97; N, 13.72; O, 23.50; S, 31.40. Found: C, 29.43; H, 1.88; N, 13.74; O, 23.78; S, 31.27. ^1H NMR (400 MHz, DMSO-d_6) δ 8.3 (br s, 2H, NH_2), 8.1 (br s, 2H, NH_2); EI-MS *m*/*z* 204 ($M^{\bullet+}$, 85%).

Electrocrystallization Experiments. Compound **1** (5 mg) was oxidized in the presence of the tetra-*n*-butylammonium salt of the desired counteranion (50 mg) in a 1/1 mixture (12 mL) of freshly distilled CH_3CN and THF. The electrocrystallization was carried out in two-compartment cells with platinum wires (l = 2 cm, ϕ = 1 mm) at constant current (0.5 μA) at 25 °C.[12]

Crystal Structure Analysis. Data collection was carried out at 293 K on a Stoe-IPDS diffractometer with graphite-monochromated Mo $KL_{2,3}$ radiation (λ = 0.710 69 Å). The data were processed with the set of programs from STOE.[16] An absorption correction was applied for $\mathbf{1}_2HSO_4$, $\mathbf{1}_2ClO_4$, and $\mathbf{1}_2Mo_6Cl_{14}$ using numerical procedures based on face indexing (FACEIT, STOE). Structures were solved by direct methods using SHELXS-86 and refined by the full matrix least-squares method on F^2, using SHELXL-93 (G. M. Sheldrick, University of Göttingen, 1993) with anisotropic thermal parameters for all non-hydrogen atoms. The hydrogen atoms were introduced at calculated positions and not refined (riding model). In **1**, the carbon atoms of the ethylenedithio bridge are disordered over two positions and have been refined with isotropic thermal parameters. In $\mathbf{1}_2HSO_4$ and $\mathbf{1}_2ClO_4$, several oxygen atoms of the anions show disorder and have been refined with isotropic parameters. Details of data collection and structure refinements are given in Table 1.

Band Structure Calculations. The tight-binding band structure calculations were based upon the effective one-electron Hamiltonian of the extended Hückel method.[17] The off-diagonal matrix elements of the Hamiltonian were calculated according to the modified Wolfsberg−Helmholz formula.[18] All valence electrons were explicitly taken into account in the calculations, and the basis set consisted of double-ζ Slater-type orbitals for C, N, O, and S and single-ζ Slater-type orbitals for H. The exponents, contraction coefficients, and atomic parameters for C, S, and H were taken from previous work.[19] Those used for N and O were 2.261, 1.424, 0.7297, 0.3455, and −26.0 eV for N 2s, 3.249, 1.499, 0.2881, 0.7783, and −13.4 eV for N 2p, 2.688, 1.675, 0.7076, 0.3745, and −32.3 eV for O 2s, and 3.694, 1.658, 0.3322, 0.7448, and −14.8 eV for O 2p.

Transport Measurements. The temperature dependence of the electrical conductivity was deduced from a four-probe resistance measurement, with a 1 μA dc current between 300 and 160 K, and from a conductance measurement with a dc voltage of 10 V at lower temperature.

Results and Discussion

A Robust and Adaptable Hydrogen-Bond Network in Single-Component Solids 1 and 2. EDT-TTF-$(CONH_2)_2$, **1**, was prepared (Scheme 1) by applying the protocol described by Bryce and co-workers[20] for the preparation of TTF-$(CONH_2)_2$. Reaction of EDT-TTF-$(CO_2Me)_2$ [15] with ammonia

(13) Etter, M. *Acc. Chem. Res.* **1990**, *23*, 120−126.
(14) Neilands, O. Y.; Valters, R. A.; Putikis, G. G.; Tilika, V. Z.; Edzhinya, A. S. *Chem. Heterocycl. Comp.* **1992**, 1079.
(15) Blanchard, P.; Sallé, M.; Duguay, G.; Jubault, M.; Gorgues, A. *Tetrahedron Lett.* **1992**, *33*, 19, 2685−2688.
(16) Stoe-IPDS Software manual V2.87, December 1997, STOE, Darmstadt, Germany.
(17) Whangbo, M.-H.; Hoffmann, R. *J. Am. Chem Soc.* **1978**, *100*, 6093−6098.
(18) Ammeter, J. H.; Bürgi, H.-B.; Thibeault, J.; Hoffmann, R. *J. Am. Chem Soc.* **1978**, *100*, 3686−3692.
(19) Pénicaud, A.; Boubekeur, K.; Batail, P.; Canadell, E.; Auban-Senzier, P.; Jérome, D. *J. Am. Chem. Soc.* **1993**, *115*, 4101−4112.
(20) Batsanov, A. S.; Bryce, M. R.; Heaton, J. N.; Moore, A. J.; Skabara, P. J.; Howard, J. A. K.; Orti, E.; Viruela, P. M.; Viruela, R. *J. Mater. Chem.* **1995**, *5*, 1689−1696.

Table 1. Crystallographic and Structure Refinement Data

	1	**2**	**1**$_2$HSO$_4$	**1**$_2$ClO$_4$	**1**$_2$ReO$_4$	**1**$_2$AsF$_6$	**1**$_2$Mo$_6$Cl$_{14}$
crystal system	monoclinic	triclinic	monoclinic	monoclinic	monoclinic	monoclinic	triclinic
space group	$P2_1/n$	P-1	$P2_1/c$	$P2_1/c$	$P2_1/c$	$P2_1/c$	P-1
a/Å	5.1518(4)	5.8330(16)	15.1947(9)	15.3700(12)	15.5632(15)	15.7167(17)	8.9713(10)
b/Å	36.4871(33)	7.4593(19)	12.2388(9)	12.3553(13)	12.2625(7)	12.4203(14)	12.4561(14)
c/Å	7.9179(6)	9.197(3)	17.1149(11)	16.8756(13)	16.9346(15)	17.1879(16)	12.7006(15)
α/deg		104.32(3)					114.258(13)
β/deg	99.987(10)	98.85(3)	99.799(7)	98.138(9)	97.624(11)	97.905(12)	105.477(14)
γ/deg		105.09(3)					92.126(14)
V/Å^3	1465.8(3)	364.0(2)	3136.4(4)	3172.4(4)	3203.3(4)	3323.3(4)	1229.5(2)
Z	4	2	4	4			1
μ/mm^{-1}	0.932	0.693	0.956	0.963			2.792
$I > 2\sigma(I)$	1430	1057	3677	2827			3325
parameters	181	109	406	406			265
R_{int}	0.061	0.039	0.060	0.069			0.034
S	0.69	0.95	0.79	0.69			0.88
R_1	0.0354	0.0265	0.0346	0.0373			0.0224
wR_2	0.0684	0.0658	0.0593	0.0757			0.0462

Scheme 1

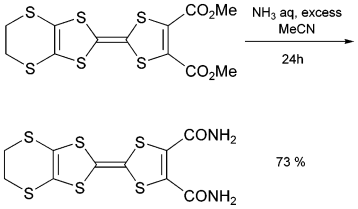

in aqueous solution affords **1** with 73% yield. Compound **1** displays two reversible waves in cyclic voltammetry [$E_{1/2}^1$ = 0.73 V and $E_{1/2}^1$ = 0.96 V vs SCE in THF, 0.05 M (n-Bu$_4$N)-PF$_6$], indicating a donor character comparable to that of BEDT-TTF [bis(ethylenedithio)tetrathiafulvalene] (0.70 and 0.95 V in the same conditions). ^{1}H NMR of a DMSO-d_6 solution of **1** reveals the presence of two peaks for the four amide N−Hs (see Experimental Section). This indicates that an intramolecular hydrogen bond exists in solution but the rotation at room temperature around the C−N bond is too fast to distinguish the hydrogen atoms belonging to a -NH$_2$ group.

In the solid state, **1** adopts a conformation closed with an intramolecular hydrogen bond (Figure 1), also observed for several secondary diamide analogues.[21] The molecules assemble into sheets forming the *ac* plane. Note that the hydrophilic−hydrophobic segregation at the interface between adjacent sheets along the *b* axis results from either self-complementary amide···amide interactions or from adjacent ethylenedithio bridges, a consequence of the formation of the hydrogen-bond network depicted in Figure 1 and characterized further in Table 2. Infinite puckered ribbons are constructed out of a sequence of three-, four-, seven-, and eight-membered homomeric, self-complementary centrosymmetrical amide···amide ring motifs (Figure 1), as expected for diamides.[3] As exemplified in Figure 1, the N2−H2B···O2 hydrogen bond connects the ribbons along the *a* axis. This results in the formation of a slab of the β'-type.[22] The latter, one of several characteristic layer topologies of two-dimensional radical cation salts, was, to the best of our knowledge, only identified once before in a monocomponent molecular solid, EDT-TTF-CONMe$_2$.[9] The present intermolecular hydrogen-bond pattern is reminiscent of the formation of tapes in 2-benzimidazolones.[23] In the spirit of Whitesides and co-workers,[23] who studied the susceptibility of this tape motif to be perturbed by the steric demand of bulky substituents, we took this opportunity to analyze the pattern of association in the solid state of the dithiolone **2**[14] and determined its crystal structure. Remarkably, the hydrogen-bond network in crystals of **2** is almost identical to that observed for **1** (Figure 2). The only difference lies in the hydrogen bonds that satisfy the N−Hs protruding out of the ribbon. In the case of **1**, the latter serves

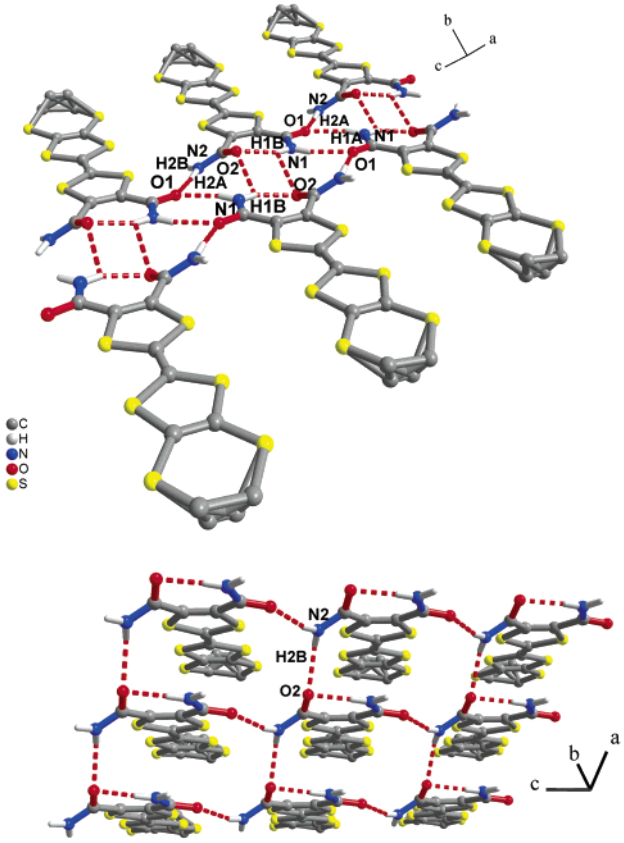

Figure 1. (a, top) Perspective onto the puckered hydrogen-bonded ribbon in **1** and (b, bottom) connection between the ribbons forming β'-type slabs. Note the two disordered conformations of the ethylenedithio bridges.

(21) (a) Beerli, R.; Rebek, J., Jr. *Tetrahedron Lett.* **1995**, *35*, 1813. (b) Baures, P. W.; Rush, J. R.; Wiznycia, A. V.; Desper, J.; Helfrich, B. A.; Beatty, A. M. *Cryst. Growth Des.* **2002**, *2*, 653−664. (c) Baudron, S. A.; Avarvari, N.; Batail, P.; Canadell, E.; Clérac, R.; Coulon, C.; Auban-Senzier, P. Manuscript in preparation.

(22) Mori, T. *Bull. Chem. Soc. Jpn.* **1998**, *71*, 2509−2526.

(23) Schwiebert, K. E.; Chin, D. N.; MacDonald, J. C.; Whitesides, G. M. *J. Am. Chem. Soc.* **1996**, *118*, 17, 4018−4029.

Table 2. N−H···O Hydrogen Bond Characteristics in **1** and **2**[a]

cmpd	inter/intra	atom label	N···O (Å)	H···O (Å)	α (deg)
1	intra	$N_1-H_{1B}\cdots O_2$	2.745(3)	1.935	156.6
1	inter	$N_1-H_{1A}\cdots O_1$	2.913(4)	2.063	169.4
1	inter	$N_1-H_{1B}\cdots O_2$	3.114(4)	2.751	107.6
1	inter	$N_2-H_{2A}\cdots O_1$	2.905(3)	2.062	166.1
1	inter	$N_2-H_{2B}\cdots O_2$	3.064(3)	2.285	150.7
2	intra	$N_1-H_{1B}\cdots O_2$	2.676(2)	1.859	157.9
2	inter	$N_1-H_{1A}\cdots O_1$	2.993(2)	2.138	172.3
2	inter	$N_1-H_{1B}\cdots O_2$	3.078(3)	2.578	118.1
2	inter	$N_2-H_{2A}\cdots O_1$	2.962(3)	2.105	175.6
2	inter	$N_2-H_{2B}\cdots O_3$	3.216(3)	2.410	115.1
CSD	intra		2.755(12)	1.988(13)	132.5(15)
CSD	inter		2.892(3)	1.913(4)	161.2(3)

[a] α refers to the N−H···O angle. A comparison with the CSD data is given.

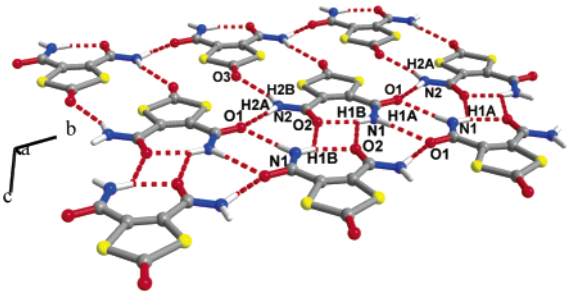

Figure 2. Perspective into the hydrogen bond net in **2**. Note the in-plane N2−H2B···O3 bond which makes for quasi-flat ribbons and a remarkable flat layer.

to connect two successive ribbons. However, the dithiolone **2** offers an additional hydrogen-bond acceptor, that is, the central C═O, which is neatly taken care of since two ribbons belonging to the same plane are now connected by the N2−H2B···O3 hydrogen bond. As a consequence, **2** is flat, unlike **1**: the torsion angles between the amide groups and the C═C are 1.7(3)° and 175.0(2)° in **2**, while they amount to 5.2(6)° and 144.2(4)° in **1**. This reveals that the hydrogen-bond network in these derivatives is robust and recurrent, yet adaptable to its environment, since it is able to adjust to the presence of an additional acceptor by a slight rotation of the amide groups.

At this point of our progress, there was good hope that this network will also be synthesized in radical cation salts of **1**, hence directing the formation of *β′*-type slabs.[22] Therefore, **1** has been engaged in electrocrystallization experiments with single-charged anions.

Preservation of the *β′*-type Slab Topology in Radical Cation Salts of 1 with Single-Charged Anions. Electrocrystallization of **1** in the presence of HSO_4^-, ClO_4^-, ReO_4^-, and AsF_6^- produces a series of salts formulated $\mathbf{1}_2X$ by resolution of their crystal structures. In sharp contrast with (EDT-TTF-$CONH_2$)$_2ReO_4$ and (EDT-TTF-$CONH_2$)$_6AsF_6$, no templating effect of the anion occurs upon engaging EDT-TTF-$(CONH_2)_2$. It can be explained by analysis of the crystal structure of the present series. Crystal structures of $\mathbf{1}_2HSO_4$ and $\mathbf{1}_2ClO_4$ were solved at 293 K, while for $\mathbf{1}_2ReO_4$ and $\mathbf{1}_2AsF_6$ only the unit cell parameters have been determined (Table 1). All phases crystallize in the monoclinic system, space group $P2_1/c$ with two EDT-TTF-$(CONH_2)_2$ molecules and one disordered anion in the asymmetric unit (Figure 3). The slabs are of the *β′*-type, as expected. The anions are intercalated between these slabs. Again, the global interfacial hydrogen-bond net geometry is that of an infinite puckered ribbon built on homomeric, self-

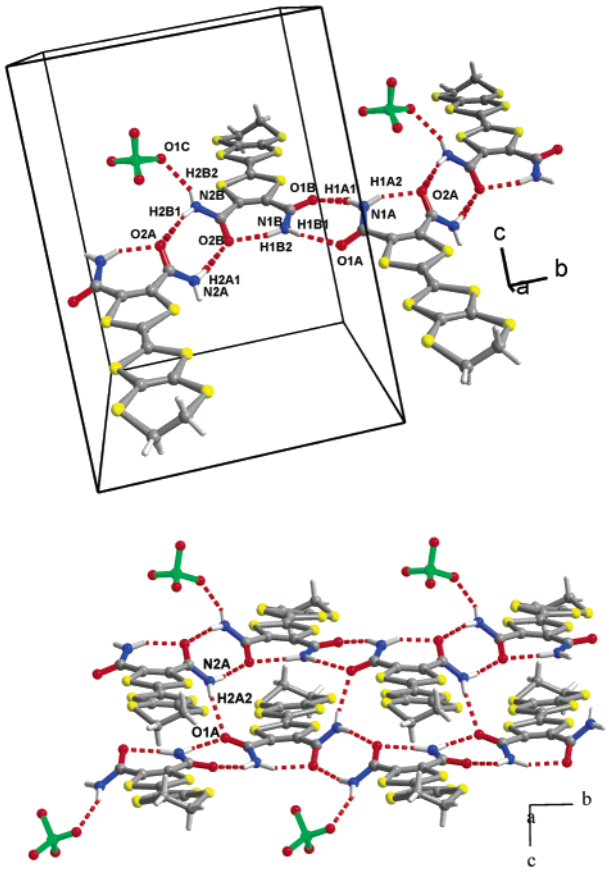

Figure 3. (a, top) Perspective onto the hydrogen-bonded ribbon in $\mathbf{1}_2ClO_4$. Note the local torsion angles and geometry of the amide groups that make for the curvature and shape of the ribbon. N−H···O hydrogen-bond lengths (angstroms) and angles (degrees) within the two unique amide···amide, intra- and intermolecular ring motifs are as follows for $\mathbf{1}_2ClO_4$ [and in brackets for $\mathbf{1}_2HSO_4$]: $N_{1A}-H_{1A1}\cdots O_{1B}$, 2.924(4), 164 [2.915(3), 167]; $N_{1A}-H_{1A2}\cdots O_{2A}$, 2.789(4), 155 [2.758(3), 158]; $N_{2A}-H_{2A1}\cdots O_{2B}$, 2.847(4), 169 [2.836(4), 172]; $N_{2A}-H_{2A2}\cdots O_{1A}$, 2.966(5), 151 [3.042(3), 143]; $N_{1B}-H_{1B1}\cdots O_{1A}$, 3.029(4), 166 [3.120(3), 170]; $N_{1B}-H_{1B2}\cdots O_{2B}$, 2.763(4), 153 [2.756(3), 153]; $N_{2B}-H_{2B1}\cdots O_{2A}$, 2.992(4), 167 [3.040(3), 165]; $N_{2B}-H_{2B2}\cdots O_{3C}$, 2.992(4), 153 [2.885(4), 153]. (b, bottom) Pattern of interribbon connectivity across N2A−H2A···O1A, represented here for $\mathbf{1}_2ClO_4$. Note that only one of the two disordered conformations of the ethylenedithio groups and ClO_4^- has been represented.

complementary, and centrosymmetrical amide···amide ring motifs (Figure 3a). Once again the N−H protruding from the ribbon are playing an important role. One of them is involved in a hydrogen bond with the anion while the other is connecting two ribbons (Figure 3b) as in the monocomponent solid **1**. Therefore, the absence of structural directing effect of the anion in these series is clearly due to the preeminence of the hydrogen-bonded network involving the *π*-donors. We then conclude that the functionality of this *o*-bis(amide)-appended TTF derivative in the $\mathbf{1}_2X$ series relies on its ability to form a cooperative sequence of eight-, seven-, and eight-membered hydrogen-bonded amide···amide ring motifs (Figure 3) and is therefore expressed primarily at the organic−organic interface. The hydrogen-bond pattern and N−H···O hydrogen-bond characteristics are quite similar for $\mathbf{1}_2HSO_4$ and $\mathbf{1}_2ClO_4$, which, at first glance, makes for virtually indistinguishable ribbon conformations and relative donor molecule orientations. An analysis of the torsion angles of the two amide groups (Table 3) reveals, however, slight differences in their local geometry. Hence, the ribbons pick up different local curvatures that are likely to

Table 3. Torsion Angles for the Two Amide Groups in $\mathbf{1}_2HSO_4$ and $\mathbf{1}_2ClO_4$[a]

	$\mathbf{1}_2ClO_4$		$\mathbf{1}_2HSO_4$	
	$N_1C_1C_2C_3$	$C_2C_3C_4N_2$	$N_1C_1C_2C_3$	$C_2C_3C_4N_2$
molecule A	−27.4(7)	−140.7(5)	−19.9(5)	−145.3(3)
molecule B	10.3(8)	141.3(4)	13.8(5)	140.7(3)

[a] Torsion angles are given in degrees.

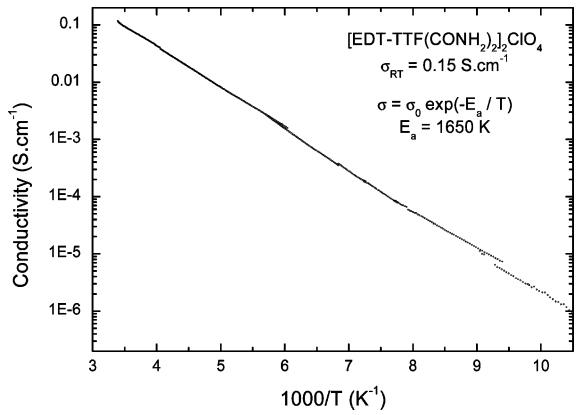

Figure 4. Electrical conductivity of $\mathbf{1}_2ClO_4$ plotted versus reciprocal temperature in order to show the activated temperature dependence.

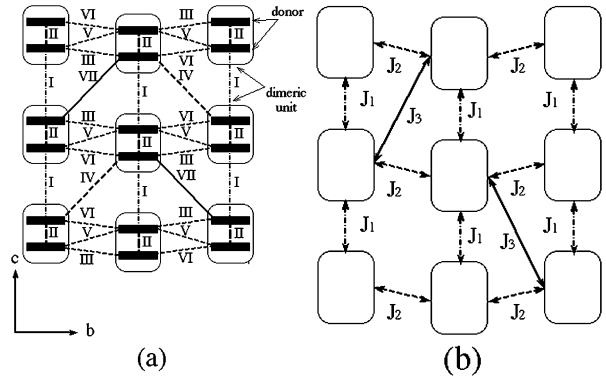

Figure 5. (a) Schematic view of the donor layers showing the seven different types of donor···donor intermolecular interactions used to estimate the interdimer magnetic interactions shown in (b).

modulate their shape, between $\mathbf{1}_2HSO_4$ and $\mathbf{1}_2ClO_4$ and throughout the whole series for that matter.

Careful bond length analysis indicates that the two independent donor molecules in the unit cell carry the same charge, hence $\mathbf{1}_2HSO_4$ and $\mathbf{1}_2ClO_4$ are mixed-valence salts. The temperature dependence of the electrical conductivity measured on $\mathbf{1}_2ClO_4$ along the long axis of a needle-shaped single crystal elongated along *c* (see Figures 3a and 5a) is depicted in Figure 4. The conductivity reaches a sizable value of 0.15 S·cm^{-1} at room temperature, and the linear variation of log σ versus T^{-1} gives an activation energy of 1650 K.

Subtle Differences in HOMO···HOMO Interactions within the β′-Topology. The donor layers of these salts contain two different donors (with very similar HOMO energies) and seven different types of donor···donor interactions (labeled I−VII in Figure 5). Interactions I and II are associated with the stacks, and interactions III−VII are interstack interactions. Every donor is implicated in two intrastack and four interstack interactions. To have a hint of the relative strength of the HOMO−HOMO interactions in these salts with respect to those of other β′-type layers reported in the literature, we have calculated the HOMO−HOMO interaction energies ($\beta_{HOMO-HOMO}$)[24] associated with these interactions. The absolute values of the $\beta_{HOMO-HOMO}$ as well as the associated S···S intermolecular contacts shorter than 4.0 Å for the different donor···donor interactions of salts $\mathbf{1}_2HSO_4$ and $\mathbf{1}_2ClO_4$ are reported in Table 4. Although there are differences in detail, the overall picture is very similar. When these values are compared with those for typical β′-type salts such as β′-(BEDT-TTF)$_2$ICl$_2$,[25] there is a clear difference in what concerns the intrastack interactions. In all β′ salts there is a clear dimerization as measured by the large difference in the $\beta_{HOMO-HOMO}$ values for the two intrastack interactions. However, whereas in the latter salt the smaller of the two intrastack interactions (0.522 and 0.014 eV)[25] is extremely weak, in $\mathbf{1}_2HSO_4$ and $\mathbf{1}_2ClO_4$ it clearly remains the smaller of the two interactions but at the same time it is now far from negligible (0.666 and 0.166 for $\mathbf{1}_2HSO_4$ as well as 0.639 and 0.164 for $\mathbf{1}_2ClO_4$). The interstack interactions are more similar, although slightly weaker [for instance, in β′-(BEDT-TTF)$_2$ICl$_2$ the four different interactions are associated with values of 0.198, 0.089, 0.057, and 0.057].[25] Both facts, the greater strength of the small interaction along the stacks and the weaker interstack interactions, cooperate in making the present β′ salts more two-dimensional than the prototypical β′-(BEDT-TTF)$_2$ICl$_2$[25] as far as the HOMO−HOMO interactions are concerned. In a certain way, the interactions in the present salts are between those typical of the semiconducting β′- and metallic β-type salts of BEDT-TTF[24a,25] although still remaining closer to those of the β′ salts. It is clear that the pattern of HOMO−HOMO interactions in β′ salts is far from uniform [for instance, the series of salts (X$_2$-EDT-TTF)$_2$Y (X = Br, Y = IBr$_2$, I$_3$; X = I, Y = I$_3$)[27] provides for a still different variation], and thus the use of appropriate substituents could lead to some control over the physical properties of this class of salts.

Table 4. Absolute Values of the $\beta_{HOMO-HOMO}$ Interaction Energies and Associated S···S Intermolecular Contacts Shorter than 4.0 Å for the Different Donor···Donor Interactions in $\mathbf{1}_2HSO_4$ and $\mathbf{1}_2ClO_4$

interaction[b]	S···S distances/Å	$\beta_{HOMO-HOMO}$/eV
I	3.863 [3.899]	0.1663 [0.1645]
II	3.576, 3.577, 3.646, 3.662 [3.565, 3.616, 3.628, 3.690]	0.6659 [0.6391]
III	3.503, 3.708 [3.526, 3.714]	0.0342 [0.0314]
IV	3.402 (×2), 3.906 [3.450 (×2), 3.978]	0.0186 [0.0042]
V	3.509, 3.637, 3.870 [3.642, 3.658]	0.0250 [0.0229]
VI	3.509, 3.561, 3.703 [3.447, 3.602, 3.710]	0.0532 [0.0454]
VII	3.667 (×2) [3.737 (×2)]	0.1493 [0.1283]

[a] Values for $\mathbf{1}_2HSO_4$ are listed first; values for $\mathbf{1}_2ClO_4$ follow in brackets. [b] See Figure 5a for labeling.

(24) (a) Whangbo, M.-H.; Williams, J. M.; Leung, P. C. W.; Beno, M. A.; Emge, T. J.; Wang, H. H. *Inorg. Chem.* **1985**, *24*, 3500−3502. (b) Note that although there can be small differences in details, the $\beta_{HOMO-HOMO}$ interaction energies and the associated transfer integrals (*t*, see later) are obviously related and have the same physical meaning. However, because overlap is explicitly included in extended Hückel calculations, the absolute values of β are somewhat larger than those of t. We use the β values here because it facilitates the comparison with other calculations for β′ salts already reported in the literature. However, when discussing the magnetic properties the *t* values are more appropriate.
(25) Emge, T. J.; Wang, H. H.; Leung, P. C. W.; Rust, P. R.; Cook, J. D.; Jackson, P. L.; Carlson, K. D.; Williams, J. M.; Whangbo, M.-H.; Venturini, E. L.; Shirber, J. E.; Azevedo, L. J.; Ferraro, J. R. *J. Am. Chem Soc.* **1986**, *108*, 695−702.
(26) Yoneyama, N.; Miyazaki, A.; Enoki, T.; Saito, G. *Bull. Chem. Soc. Jpn* **1999**, *72*, 639−651.
(27) Domercq, B., Devic, T., Fourmigué, M., Auban-Senzier, P., Canadell, E. *J. Mater. Chem.* **2001**, *11*, 1570−1575.

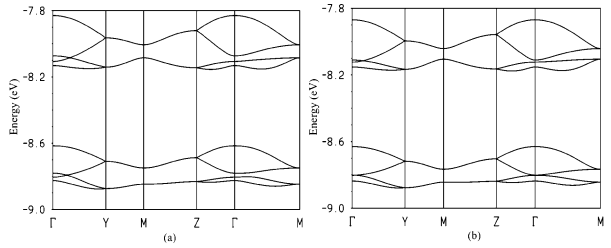

Figure 6. Calculated band structure for a donor layer of salts: (a) $\mathbf{1}_2HSO_4$ and (b) $\mathbf{1}_2ClO_4$, where $\Gamma = (0, 0)$, $Y = (b^*/2, 0)$, $Z = (0, c^*/2)$, and $M = (b^*/2, c^*/2)$.

The calculated band structures for the donor layers of $\mathbf{1}_2HSO_4$ and $\mathbf{1}_2ClO_4$ are reported in Figure 6. Since there are eight different donors per repeat unit within the layer, there are eight bands mainly built from the HOMO of **1**. These bands are split in two groups of four bands, something which is a consequence of the strong dimerization along the stacks direction. The differences between the two band structures are small. However, as expected from the slightly different values of the $\beta_{HOMO-HOMO}$ interaction energies compared in Table 4, these differences indeed exist and we note that they will turn out to be of paramount importance when it comes to understanding the susceptibility data. Because of the stoichiometry, the upper group of four bands must contain four holes. This group of four bands contains a pair of flat bands and a pair of more dispersive and isotropic bands. The two different types of bands slightly overlap (see for instance the region around the Γ point in Figure 6). As a consequence, the density of states (DOS) of these salts results from the superposition of two quite different contributions associated with the two types of bands. The region of the DOS that may be relevant to understanding the transport properties (see next section) is just that around the superposition of the two contributions. It is precisely that region which is the most affected by the small structural changes for the different $\mathbf{1}_2X$ salts. The possible relevance of these observations in understanding the transport properties of the $\mathbf{1}_2X$ salts is analyzed in detail in the following section.

Singular Magnetic Behavior for *β′* Salts. The magnetic behavior of [EDT-TTF-$(CONH_2)_2$]$_2ReO_4$ (21.03 mg) and [EDT-TTF-$(CONH_2)_2$]$_2ClO_4$ (15.79 mg) has been studied by use of a SQUID magnetometer on polycrystalline samples. The raw data have been corrected from the orbital diamagnetism ($\chi_{dia} = -2 \times 10^{-4}$ emu mol^{-1}) and from a small amount of ferromagnetic impurities. The temperature dependence of the resulting spin susceptibility is given in Figure 7. For both salts, a broad maximum is observed at low temperature (40 and 60 K, respectively) and a further increase of the susceptibility is found below 10 K. Compared to other β'-$(BEDT\text{-}TTF)_2X$ salts, this result is rather singular and is closer to the one found for bis(methylenedithio)tetrathiafulvalene salts, $(BMDT\text{-}TTF)_2X$ (X = ClO_4, AsF_6).[26] Another striking result is the important difference in susceptibility behavior between the two salts despite similar structures. This shows that the magnetic behavior of these series is sensitive to minute structural adjustments. These two points will be developed in the following discussion.

As mentioned in the Experimental Section, the crystal structures of $\mathbf{1}_2HSO_4$ and $\mathbf{1}_2ClO_4$ are similar to the one reported for β'-$(BEDT\text{-}TTF)_2X$ salts. For X = ICl_2 and $AuCl_2$, the compounds have been studied in detail and present a low-temperature antiferromagnetic ground state.[26,28] These materials

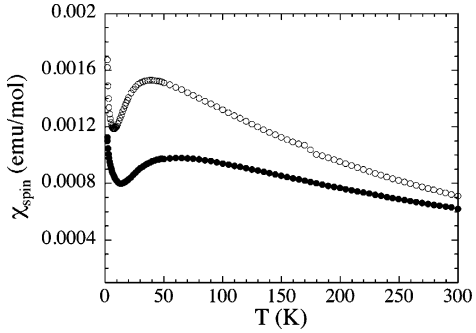

Figure 7. Temperature dependence of the spin susceptibility deduced from the magnetometer measurements on a powder sample of [EDT-TTF-$(CONH_2)_2$]$_2ClO_4$ for an applied dc field of 1000 Oe (●) and [EDT-TTF-$(CONH_2)_2$]$_2ReO_4$ for an applied dc field of 5000 Oe (○).

have a very low electrical conductivity (typically 10^{-2} S·cm^{-1} at room temperature) and are therefore described as Mott insulators. For this reason, their magnetic properties were analyzed in the strong coupling limit where the electron−electron interaction overcomes the kinetic electronic energy. Although a higher electrical conductivity has been measured for [EDT-TTF-$(CONH_2)_2$]$_2ClO_4$, the strong coupling limit most likely remains relevant. The extreme sensitivity of the magnetic behavior to minute modifications of the ribbon curvature has been shown to be the consequence of singular features of intermolecular interactions (see Figure 5 and Table 4). It is important to note that the transfer integral data contain the information relevant to the analysis of the magnetic susceptibility regardless of the magnitude of the electron−electron interaction. Therefore, the former singular features should have particular consequences in the strong or weak coupling limit, which we now analyze.

In the weak coupling limit, the key information is the electronic DOS, which is readily deduced from the band structure calculation. As shown previously (Figure 6), the band structure consists of two groups of bands well separated by a large gap. Figure 8a gives the calculated DOS in the case of [EDT-TTF-$(CONH_2)_2$]$_2ClO_4$ (normalized per dimer, i.e., as its integral over the energy gives two electrons) for the upper band group. The Fermi energy, E_F, gives the position of the highest occupied state at $T = 0$ K and is located by the dashed line in Figure 9a. A similar result is found for [EDT-TTF-$(CONH_2)_2$]$_2$-ReO_4 with, however, a slightly different position of the Fermi level. Schematically, as discussed above, the obtained density of state is the superposition of a 1D (at lower energy) and a 2D component at higher energy. The present system is singular as the Fermi level lies at the frontier between these two contributions, i.e., in a region where the density of states is very asymmetric and strongly energy-dependent. Therefore, small modifications of the structure, which shall induce small displacements of E_F, may imply noticeable variations of the spin (Pauli) susceptibility. To probe this idea, we have calculated numerically the spin susceptibility (Figure 8b). To mimic the small structural variations among the series, we have changed the band filling. It is worth noticing that this strategy, which induces a displacement of the Fermi energy, is equivalent to imposing small modifications of the DOS energy dependence.[29] From Figure 8b, it is clear that the spin susceptibility is strongly

(28) Coulon, C.; Laversanne, R.; Amiell, J.; Delhaes, P. *J. Phys. C.: Solid State Phys.* **1986**, *19*, L753−L758.

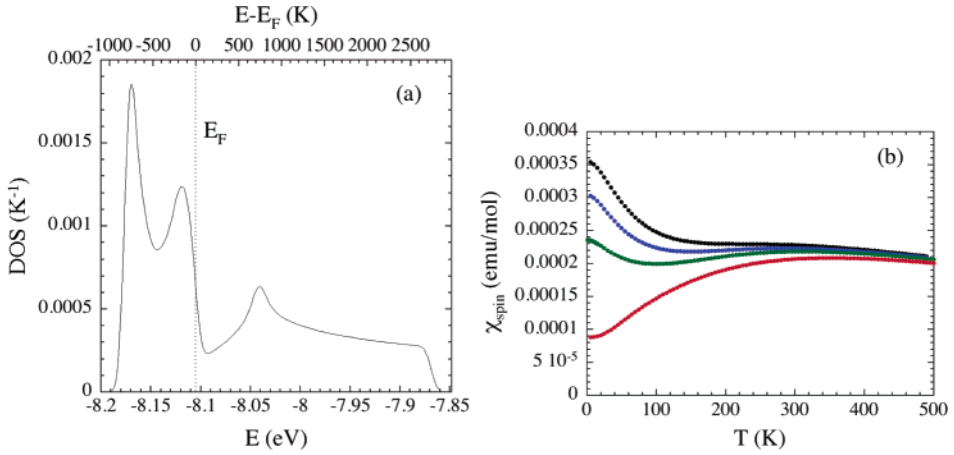

Figure 8. (a) Density of states (DOS) calculated for [EDT-TTF(CONH$_2$)$_2$]$_2$ClO$_4$. (b) Spin susceptibility of [EDT-TTF(CONH$_2$)$_2$]$_2$ClO$_4$ deduced from the DOS presented in panel a at band fillings $n = 0.96$, 0.98, 1, and 1.05 (shown in black, blue, green, and red, respectively).

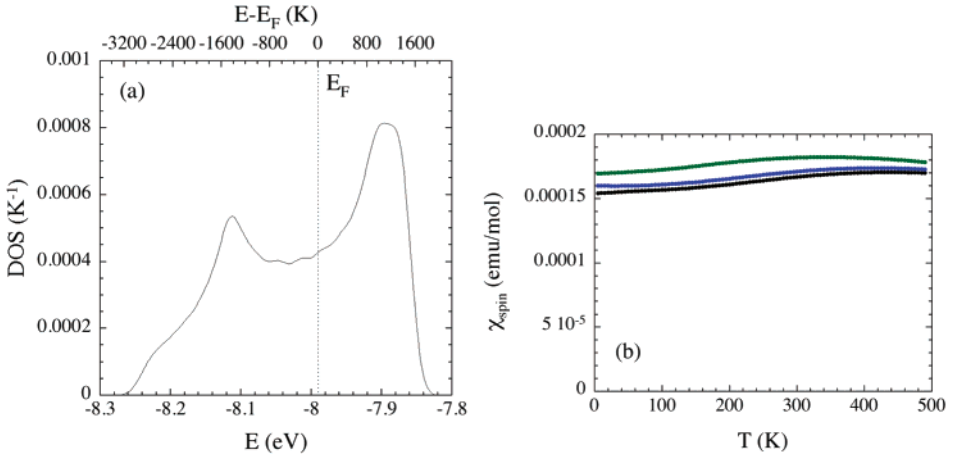

Figure 9. (a) Density of states (DOS) calculated for β′-[BEDT-TTF]$_2$ICl$_2$. (b) Spin susceptibility of β′-[BEDT-TTF]$_2$ICl$_2$ deduced from the previous DOS at $n = 0.95$, 1, and 1.05 (shown in black, blue, and green, respectively). Note that the scale of susceptibility axis has been enhanced compared to that in Figure 7.

dependent on the position of the Fermi level. Moreover, for $n = 1$, a broad maximum is observed at about 300 K, followed by a further increase at lower temperature. Thus, the experimental data are qualitatively reproduced, although both the position of the maximum and the absolute value of the susceptibility are different. The larger experimental value observed for the latter is the manifestation of significant electron interactions.[30]

Likewise, significant electron interactions make for the observed temperature dependence of the electrical conductivity, which shows an activation energy (i.e., a correlation gap) instead of metallic behavior. In any case, this first part of the discussion already reveals the singular character of these compounds. In fact, a similar approach leads to a completely different discussion for standard β′-salts such as β′-(BEDT-TTF)$_2$ ICl$_2$. Figure 9a gives the corresponding density of states. The Fermi level is now located at an energy where the DOS varies only smoothly and the corresponding spin susceptibility (shown in Figure 9b) is almost constant and nearly independent of the band filling.

To deepen this discussion, it should be noted that the spin susceptibility can also be obtained by introducing electron interactions as a perturbation (considering that they remain small compared to the Fermi energy). In that case, the temperature of the susceptibility maximum remains roughly the same[30b,31] and we therefore consider the other simple limit, where electron−electron interactions are assumed to be dominant. In that case, since the band structure is no longer relevant, the transfer integrals between donors should be used to estimate the different exchange interactions between the dimeric units.[31,28] Figure 5a shows the 2D network relevant for this discussion (transfer integrals are negligible in the third direction). Table 5 gives the corresponding values of the different transfer integrals for [EDT-TTF-(CONH$_2$)$_2$]$_2$HSO$_4$ and [EDT-TTF-(CONH$_2$)$_2$]$_2$ClO$_4$. Note that VI is particularly sensitive to small modifications of the structure. The corresponding diagram showing the magnetic interactions between the dimeric units is given in Figure 5b, neglecting the weak transfer integral labeled IV in Figure 5a. There are essentially three different exchange energies. Two of

(29) The first step of the calculation is the determination of the temperature dependence of the chemical potential, μ, by use of the equation; $n = \int_{E_{min}}^{E_{max}} [D(E)\, dE]/[e^{(E-\mu)/k_BT} + 1]$, where n is the band filling ($n = 1$ for the half-filled case), $D(E)$ is the electronic density of states, and E_{min} and E_{max} are the energies at the band limit. By definition, the 0 K value of μ is the Fermi energy E_F. The second step is the calculation of the spin susceptibility per dimer: $\chi_{spin} = [\mu_B{}^2]/[k_BT] \int_{E_{spin}}^{E_{max}} [D(E)e^{(E-\mu)/k_BT}\, dE]/[(e^{(E-\mu)/k_BT} + 1)^2]$. The corresponding result, normalized per mole, is given in Figure 8b.

(30) (a) Torrance, J. B.; Tomkiewicz, Y.; Silverman, B. D. *Phys. Rev.* **1977**, *B15*, 4738−4749. (b) Mazumdar, S.; Dixit, S. N. *Phys. Rev.* **1986**, *B34*, 3683−3699.

(31) Nélisse, H.; Bourbonnais, C.; Touchette, H.; Vilk, H. M.; Tremblay, A. M. S. *Eur. Phys. J. B* **1999**, *12*, 351−365.

Table 5. Calculated Transfer Integrals for $[EDT\text{-}TTF(CONH_2)_2]_2[X]$

	t (meV)	
interactions	X = HSO_4	X = ClO_4
I	76	62
II	381	352
III	3	<1
IV	4	3
V	−22	−19
VI	16	<1
VII	−101	−86

them, J_1 and J_3, result from only one transfer integral and are known to be antiferromagnetic.[33] On the other hand, the interaction J_2 in the horizontal direction is the result of transfer integrals of opposite sign (essentially V and VI, as III is small). In that case, this interaction can be either antiferromagnetic or ferromagnetic, depending on the relative magnitude of V and VI.[32,28] The situation found in $(BEDT\text{-}TTF)_2ICl_2$ leads to a ferromagnetic J_2 and the three magnetic interactions act in unison to promote a low-temperature antiferromagnetic ground state. The situation may be different in the present salts. Although a low-temperature structure would be necessary to estimate J_2 (as VI and therefore J_2 are sensitive to small structural modifications), we note that an antiferromagnetic J_2 competes with J_1 and J_3 and the resulting frustration may explain the experimental result.[34] A similar argument has been given to explain the magnetic properties of $(BMDT\text{-}TTF)_2X$ salts.[26]

Restoring an Organic−Inorganic Interface in $\mathbf{1}_2Mo_6Cl_{14}$. To probe the adaptability of the hydrogen-bond network described above and the robustness of this construction principle of a β'-type topology to larger steric demand and charge of the anion, **1** was electrocrystallized in the presence of $[Mo_6Cl_{14}]^{2-}$, which yielded a 2:1 salt. $\mathbf{1}_2Mo_6Cl_{14}$ crystallizes in the triclinic system, space group *P*-1 with one donor molecule in general position and one cluster located on an inversion center. The donor molecules arrange in a hydrogen-bonded chain of discrete centrosymmetrical dimers. The dimers are fully oxidized according to the central C═C bond lengths of the TTF cores. Calculated intra- and interdimer $\beta_{HOMO-HOMO}$ interaction energies amount to 0.87 and 0.17 eV, respectively. Again, the hydrogen-bond network is made of the recurrent, homomeric, self-complementary, and centrosymmetrical amide···amide ring motif (Figure 10). The resulting bimolecular entity interacts with the hydrogen-bond acceptor terminal chloride ligands of $[Mo_6Cl_{14}]^{2-}$, forming another self-complementary square motif. Hence, the β'-type organization is destroyed in this salt in favor of the reconstruction of an organic−inorganic interface. It would thus be of interest to probe further the balance of these competing interfacial interactions (and the inherent robustness of the self-complementary centrosymmetrical amide···amide ring motif) by synthesizing salts with 3^- and 4^- charged anions and deciphering their structure.

(32) Laversanne, R.; Coulon, C.; Amiell, J. *Europhys. Lett.* **1986**, *2*, 401−408.
(33) Pincus, P. *Solid State Commun.* **1972**, *11*, 305.
(34) Strictly speaking, frustration only exists when the three exchange interactions are equal. However, they are already competing as soon as they are both antiferromagnetic and have similar values.

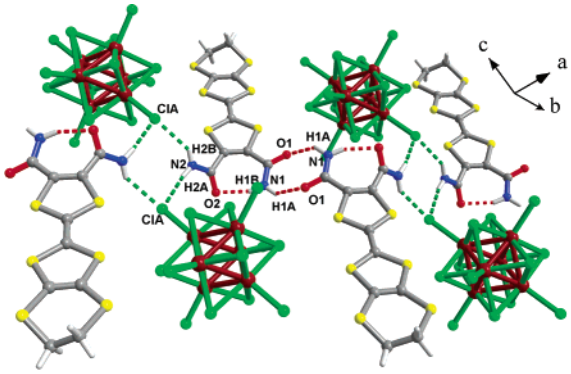

Figure 10. Hydrogen-bond network in $\mathbf{1}_2Mo_6Cl_{14}$. N−H···X hydrogen-bond lengths (angstroms) and angles (degrees): $N_1–H_{1B}\cdots O_2$, 2.787(5), 156.8; $N_1–H_{1A}\cdots O_1$, 2.986(5), 135.2; $N_2–H_{2A}\cdots Cl_A$, 3.402(3), 164.8; $N_2–H_{2B}\cdots Cl_A$, 3.285(3), 144.3.

Conclusion

In sum, the deliberate design of a series of conducting two-dimensional radical cation salts of *o*-bis(amide)-appended ethylenedithiotetrathiafulvalene, β'-$[EDT\text{-}TTF\text{-}(CONH_2)_2]X$ ($X = HSO_4^-$, ClO_4^-, ReO_4^-, or AsF_6^-), and of their parent monocomponent solids allows us to reach a level of prediction of the structure of molecular conductors. Their conductivity is activated with a sizable room-temperature conductivity of 0.15 $S\cdot cm^{-1}$ (for $X = ClO_4^-$) and a singular spin susceptibility for a β'-type salt which, in addition, changes very remarkably with the anion. The key design element is that of a recurrent, puckered ribbon constructed out of self-complementary, hydrogen-bonded amide···amide ring motifs whose minute modulations of curvature and shape throughout the series have been shown to correlate with very remarkable differences in the intrastack $\beta_{HOMO-HOMO}$ interactions energies and changes in the density of states at the Fermi level and on to important differences of spin (Pauli) susceptibility behavior in a system where electron correlations are significant. The coupled activation of structure, electron interactions, and magnetic susceptibility discovered and discussed throughout this paper is unprecedented and is seen as a genuine expression of interfacial hydrogen-bond interactions onto the collective electronic properties. It can be regarded as an important step in the development of means to direct the structure and interfere with the physics of electronic materials.

Acknowledgment. We thank the Centre National de la Recherche Scientifique, the Région des Pays de la Loire (Ph.D. grant to S.A.B.), and the Région d'Aquitaine for support. We also thank Florent Richard for assistance with calculations for Figure 8b and Jean-Charles Ricquier for his help in preparing the illustrations. This work was also supported by the joint French−Spanish Programs Picasso (1999−2000 01459 SF) and CNRS−CSIC (2000−2001 7944); DGI-Spain (Project BFM2000-1312-C02-01) and Generalitat de Catalunya (Project 2001 SGR 333).

Supporting Information Available: Tables of positional and thermal parameters, and additional crystallographic data (CIF). This information is available free of charge via the Internet at http://pubs.acs.org.

JA0356129